Gap opening of image potential state on reconstructed Ir(001) surface

Pratyay Amrit [1], Naoya Kawakami [1], Noriaki Takagi [2], Hiroshi Ishida [3], Chun-Liang Lin [1,*] and Ryuichi Arafune [4,†]

[1]*Department of Electrophysics, National Yang Ming Chiao Tung University, 1001 University Rd., Hsinchu 300, Taiwan*

[2]*Graduate School of Human and Environmental Studies, Kyoto University, Kyoto 606-8501, Japan*

[3]*College of Humanities and Sciences, Nihon University, Tokyo, Japan*

[4]*Research Center for Materials Nanoarchitectonics (MANA), National Institute for Materials Science (NIMS), 1-1 Namiki, Ibaraki 304-0044, Japan*

(Received 23 February 2025; accepted 3 June 2025; published 23 June 2025)

We have investigated the image potential states (IPSs) for the unreconstructed Ir(001)-(1×1) and the reconstructed Ir(001)-(5×1) surfaces by using two-photon photoemission spectroscopy. We reveal that the Ir(001)-(5×1) reconstructed surface covered by Xe adatoms exhibits a band gap of 100 meV, which arises from the new periodic potential created by the reconstruction, whereas no band gap was observed on the Ir(001)-(1×1) surface within the measured momentum range. The experimental results are compared with the theoretical ones obtained within density functional theory for both the clean and Xe-covered Ir(001)-(5×1) reconstructed surfaces. The planar averaged charge density distributions of the IPS for both the surfaces show that the Xe adsorption does not significantly alter the positions of charge density maxima, which rationalizes why the band gap arising from the substrate superlattice potential does not change significantly upon Xe adsorption. The agreement between the experimentally observed band gap for the IPS on the Xe-covered surface and the theoretical calculations highlights the robustness of IPS behavior under Xe adsorption.

DOI: 10.1103/46k5-fft2

I. INTRODUCTION

Surface reconstruction resulting from the rearrangement of surface atoms usually plays an important role in altering the electronic properties of materials. Experimental studies have shown that surface reconstruction affects the occupied electronic states [1–5]. However, the effect of surface reconstruction on the unoccupied states, particularly image-potential states (IPSs), remains largely unexplored. IPSs are unique surface-bound electronic states that exist near the vacuum level [6,7]. They exhibit remarkable characteristics, such as long lifetimes and free electronlike effective mass. A deeper understanding of how atomic rearrangements influence IPSs could shed light on fundamental electron dynamics at surfaces and pave the way for potential applications in devices like quantum dot transistors [8–10] and ultrafast photodetectors [11].

Previously, many studies have demonstrated the effects of adsorbates on metal surfaces and their impact on IPSs [12–21]. For example, Muller *et al.* have deposited FePc on Ag(111) and observed a strong modification of IPSs [22], indicating that IPSs can be altered by a periodic potential of the molecular array. Rather than adding additional adsorbates on the surface, a self-reconstructed surface is much more favorable to study the influence of how the rearrangement of atoms can affect the IPSs while excluding the additional charge transfer from adsorbates.

In this study, we will investigate the effect of surface reconstruction on IPSs by applying two-photon photoemission (2PPE) spectroscopy on Ir(001) surface, which forms (1×1) metastable unreconstructed and (5×1) reconstructed structures. Here, Xe atoms are used to adjust the work function of Ir(001) surface to fit the photon energy of 2PPE experiments. Our findings revealed that the IPS on the Xe-covered Ir(001)-(5×1) surface exhibits a band gap, whereas the corresponding one on the Xe-covered Ir(001)-(1×1) surface does not. The difference is attributed to the distinct reconstructions of the two surfaces, i.e., IPSs are sensitive to the variation of the potential parallel to the surface caused by the symmetry breaking. We further examined the influence of Xe adsorption on IPSs by using theoretical calculations. The size of band gap does not show significant change upon Xe adsorption, indicating that Xe primarily lowers the work function without significantly altering the unoccupied electronic states.

II. EXPERIMENTAL AND THEORETICAL METHODS

The sample preparation was performed in an ultrahigh vacuum (UHV) chamber with a base pressure of 1×10^{-10} mbar. The (5×1) reconstructed surface was prepared by the following treatments: First, the sample surface was sputtered with 1.5 keV Ar ions for 30 mins, followed by exposure to 6×10^{-8} mbar of O_2 with heating at 1220 K for 10 mins to remove the carbon impurities. O_2 reacts with the carbon impurities seg-

*Contact author: clin@nycu.edu.tw

†Contact author: arafune.ryuichi@nims.go.jp

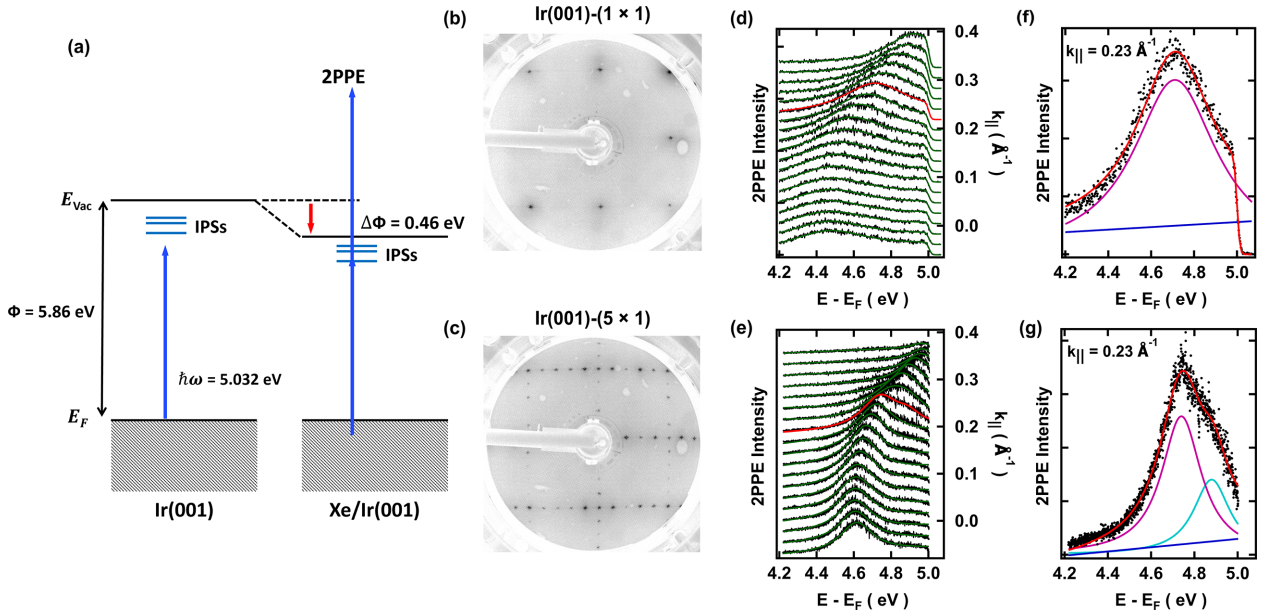

FIG. 1. (a) Schematic illustration of the 2PPE process and the role of Xe adsorption in lowering the work function, thereby enabling population of the IPSs. LEED patterns obtained with $E_b = 99.5$ eV for (b) the (1×1) surface and (c) the (5×1) surface. The series of 2PPE spectra of (d) the Xe/(1×1) and (e) the Xe/(5×1). The green and red solid curves in (d) and (e) represent the fitted curve (see text). 2PPE spectrum at $k_{||} = 0.23$ Å^{-1} for (f) the Xe/(1×1) and (g) the Xe/(5×1). Black dots represent the experimental data, and the red solid curve is the fitted curve (see text). The pink and light blue curve represent the deconvoluted peak, and the blue line is a linear baseline.

regated from the bulk and removes it from the surface [1,23–25]. Then, flash annealing in the UHV at 1420 K for 1 min results in the (5×1) reconstruction. When preparing the (1×1) metastable surface, the reconstructed (5×1) structure was eliminated by annealing at 530 K for 10 mins, followed by O_2 adsorption at 1×10^{-7} mbar. The O_2-exposed surface was then rapidly annealed in the UHV environment for 30 secs at 750 K. To completely remove the O_2 from the surface, the sample was exposed to H_2 at 1×10^{-7} mbar for 5 mins at 530 K, resulting in a clean (1×1) surface [26,27].

After the sample processing, the sample was transferred to the analysis chamber constructed of μ metal, with a base pressure better than 8×10^{-11} mbar. The sample was cooled down to ~12 K using liquid helium. The 2PPE experimental setup consisted of a Ti:sapphire laser oscillator (Coherent, Mira900) with a pulse duration of 170 fs and a repetition rate of 80 MHz, and a hemispherical electron energy analyzer (Specs GmbH, Phoibos 100) equipped with a two-dimensional detector. Ultraviolet light with an energy of 5.032 eV was generated by frequency-tripling using β-BaB_2O_4 nonlinear crystals. All the measurements were conducted using the p-polarized light, with the laser beam incident at 45° off normal to the sample surface. The photoelectrons were analyzed with the pass energy set at 5 eV. Angle-resolved measurements were made along the $\bar{\Gamma}-\bar{X}$ direction. Due to insufficient photon energy in our setup to populate the IPS, Xe was adsorbed on the sample prior to the 2PPE measurement to lower the work function by exposing the sample to 1.0×10^{-8} mbar Xe gas for 5 mins at 40 K [12,28–32]. A schematic diagram of the 2PPE process and the role of Xe adsorption in lowering the work function is illustrated in Fig. 1(a). By monitoring the work function change as a function of exposure time, we have judged that the monolayer Xe was formed. For the (5×1) surface, the work function decreased monotonically from 5.86 eV to 5.40 ± 0.03 eV over 5 mins. For the (1×1) surface, the work function decreased to 5.24 ± 0.03 eV, and after that, it did not change significantly. In this study, the coverage of Xe (θ) is defined as the ratio between the Xe atoms and underlying Ir(001)-(1×1) atoms. The monolayer of Xe corresponds to $\theta = 0.45$ from the model strucutre [24].

We performed theoretical calculations using the computer code referenced in [33] within the framework of density functional theory (DFT), combined with the embedded Green's function (EGF) technique [34] and the full-potential linearized augmented plane-wave method [35]. This approach was used to calculate the electronic structure of semi-infinite Ir(001)-(5×1) and $-(1\times1)$ surfaces [36–38]. We used the DFT-LDA exchange-correlation energy functional since DFT-GGA underestimates work functions of 5d metals typically by a few tenths of eV. Furthermore, in order to be able to reproduce IPSs, the planar average of the short-range DFT one-electron potential, $\bar{V}_{\rm eff}(z)$ with z being the surface normal coordinate, is admixed gradually with a model image potential by using an interpolation function proposed by Nekovee and Inglesfield [39],

$$V(z) = [1-\rho(z)]\bar{V}_{\rm eff}(z) + \rho(z)\left[E_V - \frac{1}{4(z-z_{im})}\right], \quad (1)$$

where E_V denotes the vacuum level, and $p(z)$ varies smoothly from 0 at $z = z_{im}$ (the image plane), to 1 at $z = z_b$ (the embedding surface on the vacuum side). The effects of the asymptotic Coulomb potential beyond z_b are incorporated by the embedding potential acting on $z = z_b$. The image plane (z_{im}) position is determined by the center of mass of the charge density induced by a weak static electric field, with the topmost Ir atom position defined as $z = 0$ [40–43].

The input data for the aforementioned EGF program is the atomic coordinates of each surface. For the clean (1×1) and (5×1) surfaces, we adopt the same atomic geometry as described in Ref. [38]. For the Xe-covered surfaces, we optimized the atomic heights of Xe adatoms relative to the Ir(001) substrate by using the VASP program [44,45]. To do so, we employed the rev-VDW-DF2 functional [46,47] to approximately account for van der Waals interactions.

III. RESULTS AND DISCUSSIONS

The low energy electron diffraction (LEED) patterns in Figs. 1(b) and 1(c) confirm the high-quality Ir(001) surfaces, with clear diffraction spots for both the (1×1) and the (5×1) surfaces. Figures 1(d) and 1(e) show a series of 2PPE spectra of the IPS ($n = 1$) for the Xe-covered Ir(001)-(1×1) [Xe/(1×1)] and the Xe-covered Ir(001)-(5×1) [Xe/(5×1)], respectively. The spectra for the Xe/(1×1) consist of a single peak across all momentum. In contrast, the spectra of the Xe/(5×1) exhibits a shoulder at $k_{||} = 0.23$ Å^{-1}, which is the first Brillouin zone (BZ) boundary in the $\bar{\Gamma} - \bar{X}$ direction for the (5×1) surface, highlighted by the red curve.

Figure 1(f) shows the spectrum for the Xe/(1×1) at $k_{||} = 0.23$ Å^{-1}. The black dots represent the experimental data, and the red curve indicates the fitted curve. The fitting was performed using the sum of the Lorentzian function (pink) and a linear baseline (blue), multiplied by the Fermi-Dirac function to account for the Fermi level cutoff. The resulting function was then convoluted with the Gaussian function that represents the instrument function. The full width at half maximum of the Gaussian function from the fitting was 30 meV. The curve was well fitted using the single Lorentzian function, confirming that there is no gap in the IPS of the Xe/(1×1). The curve at the BZ boundary for the Xe/(5×1) is plotted in Fig. 1(g). The curves are well fitted by introducing two Lorentzian functions, as shown by the pink and light blue curves. The peak positions for the pink and light blue curves are 4.75 eV and 4.85 eV, respectively, corresponding to the top and bottom of the lower and upper bands. These peak positions observed in 2PPE experiments indicate a band gap of 100 ± 10 meV. Therefore, the spectra of the Xe/(5×1) exhibit a band gap in the IPS, whereas those of Xe/(1×1) do not.

Figures 2(a) and 2(b) show the 2D band structure data of the IPS ($n = 1$) for the Xe/(1×1) and Xe/(5×1), using the maximum curvature method to highlight the curves [48]. The red dashed curve in Fig. S1 represents the parabolic fitting [49], as shown in the Supplemental Material [50]. From the fitting, the effective mass was evaluated to be the same as the mass of the free electron, indicating that the IPS retain their free-electron-like dispersion. The blue curve in Fig. S2(d) represents the band structure calculated from the Kronig-Penney (K-P) model [51]. Briefly, we assume the one-dimensional free-electron Hamiltonian including the periodic rectangular potential with a height of 0.14 eV and a width of 6.77 Å, shown in the Supplemental Material [50], which well characterizes the surface potential distribution calculated from the DFT calculations for the (5×1) surface. We obtain a 100 meV energy gap. We do not observe the spectral intensity of the folded band ($k_{||} = 0.00 - 0.20$ Å^{-1} for the upper branch and

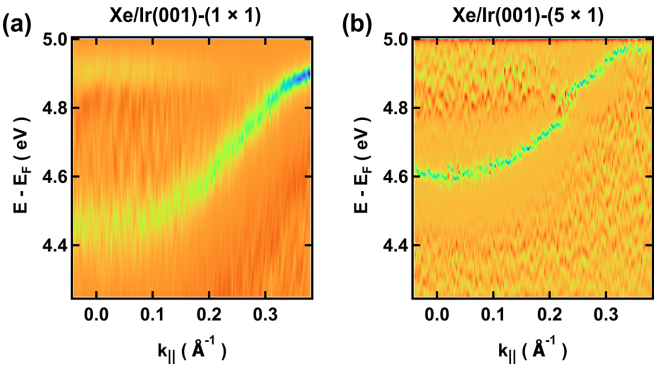

FIG. 2. 2D Band structure of the IPS for (a) the Xe/(1×1) and (b) the Xe/(5×1), measured via 2PPE at 12 K and shown using the maximum curvature method.

$k_{||} = 0.25 - 0.40$ Å^{-1} for the lower branch) for the Xe/(5×1) in Fig. 2(b). The reason is unclear, but the faint or missing spectral intensities in the other half of the folded bands are consistent with previous studies [17]. Note that, when referenced to the parabolic fit plotted in Fig. S1, the deviation of the band above $k_{||} = 0.34$ Å^{-1} in Figs. 2(a) and 2(b) are the artifacts by the maximum curvature method, which enhances the intensity change by the Fermi-Dirac distribution. Our experimental results, supported by the K-P model, provide explicit evidence that the surface potential change due to the surface reconstruction significantly influences the electronic properties of the unoccupied states, particularly the free-electron-like IPSs.

It is well known that the Xe atoms form an overlayer incommensurate with the Ir(001) surface, modifying the electronic structure by lowering the work function [28,52,53]. Besides, the Xe layer may push the IPS away from the surface, weakening the effect of potential corrugation of the reconstructed surface to the IPS. Despite these, we experimentally observed a sizable band gap at the BZ boundary of the (5×1) lattice. To investigate the impact of Xe adsorption on the IPSs on both (1×1) and (5×1) surfaces, we performed DFT calculations, including the image potential correction [54].

Figure 3(a) shows the relaxed structural model for the clean (5×1) surface. The top view highlights the quasihexagonal top layer formed by (5×1) reconstruction [27,55–57], with the unit cell marked by a black rectangle. The side view shows the corrugation of the topmost layer [27,38]. Figure 3(b) shows the DFT calculated band structure of the IPS for the (5×1) surface along the $\bar{\Gamma}$- $\bar{X}$ direction, where we used a band unfolding method [58] to calculate the band structure beyond the $\bar{X}$ point. The calculated work function is 5.63 eV, and the energy of the IPS ($n = 1$) at the $\bar{\Gamma}$ point is 4.95 eV. A 60 meV band gap, highlighted in the zoomed-in image, is observed, resulting from surface reconstruction. In contrast, no band gap is observed in the IPS for the (1×1) surface, as shown in Fig. 3(c). These results are in good agreement with the experimental results and the K-P model fitting, as discussed above.

To elucidate whether the band gap of the clean reconstructed surface is affected by the Xe layer or not, we performed the DFT calculations for the Xe/(5×1) surface.

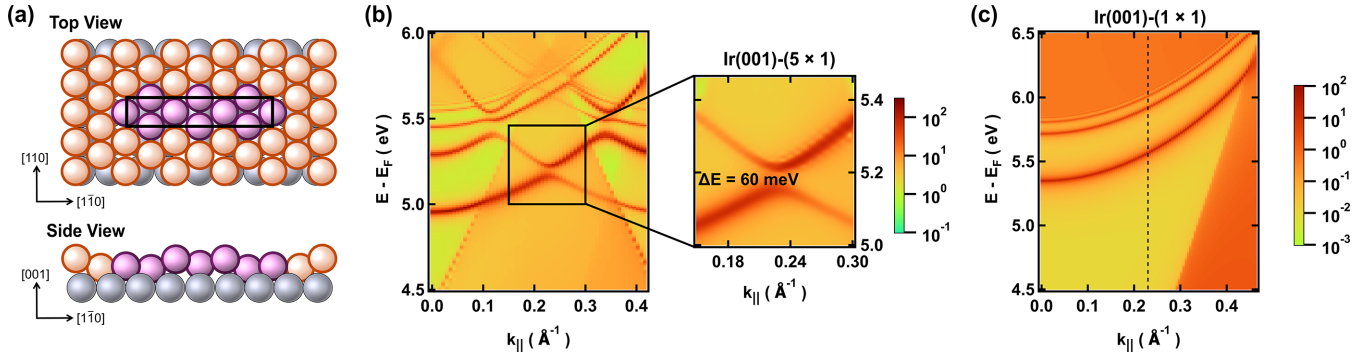

FIG. 3. (a) Ball model showing the top and side view for the clean (5×1) reconstructed surface, with the unit cell highlighted by a black rectangle box. Calculated band structure for (b) the clean (5×1) reconstructed surface and (c) the clean (1×1) unreconstructed surface, determined along the $\bar{\Gamma}$-$\bar{X}$ direction. The band structures are shown in logarithmic intensity. The zoomed-in area in (b) highlights the band gap present.

Since the monolayer Xe is incommensurate with the underlying (5×1) surface, unfortunately, it is not feasible for DFT calculation. Instead, we used a commensurate (5×2) structure [Xe/(5×2)] to investigate the effect of Xe adsorption, corresponding to $\theta = 0.3$. Figure 4(a) shows the relaxed structural model for the top and side view of the Xe/(5×2) surface, with Xe atoms (green) and the unit cell (black rectangle). The Xe atoms adsorb on top of the Ir atoms with the Ir-Xe interplane distance of 3.39 Å.

Figure 4(b) shows the DFT calculated band structure of the IPS for the Xe/(5×2) surface. The work function calculated for the Xe/(5×2) surface is 4.74 eV. On comparing with the Xe-free (5×1) surface, the work function is 0.89 eV lower on the Xe/(5×2) surface. The energy of the IPS ($n = 1$) at the $\bar{\Gamma}$ point is 3.95 eV, which is 0.10 eV deeper than that on the Xe-free (5×1) surface. A band gap, highlighted in the zoomed-in image, of 45 meV is observed, which is 15 meV smaller than that of the Xe-free (5×1) surface. These results show that the band gap persists even after Xe adsorption. As for a Xe-covered unreconstructed surface, we considered a $(\sqrt{2}\times\sqrt{2})$ lattice of Xe adatoms on unreconstructed Ir(001) [Xe/$(\sqrt{2}\times\sqrt{2})$] with the coverage of $\theta = 0.5$ [59]. The work function, calculated from DFT, is 4.99 eV, which is 0.92 eV lower than that of the Xe-free (1×1) surface. The energy of the IPS ($n = 1$) at the $\bar{\Gamma}$ point is 4.36 eV. The Xe/Ir(001)-$(\sqrt{2}\times\sqrt{2})$ surface, shown in Fig. 4(c), does not exhibit a band gap. This suggests that the surface reconstruction is the dominant factor in band gap formation in the IPS, even in the presence of the Xe layer.

To further understand the effect of the Xe adsorption on the IPS, we examined the change in the charge density distribution of the IPS ($n = 1$) near the surface. The blue curve in Fig. 5(a) shows the planar averaged charge density distribution of the IPS at the $\bar{\Gamma}$ point for the Xe-free (1×1) surface, with $z = 0$ corresponding to the outermost Ir atoms (Ir_1, indicated by purple triangle). The blue dashed line at 1.64 Å indicates the z_{im} position obtained from the DFT calculations for the Xe-free (1×1) surface. The red curve in Fig. 5(a) shows the charge density distribution of the IPS for the Xe/$(\sqrt{2}\times\sqrt{2})$ with the outermost Xe atom (green triangle). The z_{im} (red dashed line) position obtained from the calculation is −0.57 Å inside the Xe atomic layer. The z_{im} position in the interior of the Xe layer is particularly interesting and we will discuss it later. Despite the Xe layer being 3.39 Å above the topmost Ir_1 atom, the maximum IPS charge density occurs nearly at the same positions in both surfaces: $z = 5.62$ Å for Xe free (1×1) and $z = 6.15$ Å for Xe/$(\sqrt{2}\times\sqrt{2})$. This similarity in the maxima positions of charge density suggests that Xe adsorption does not

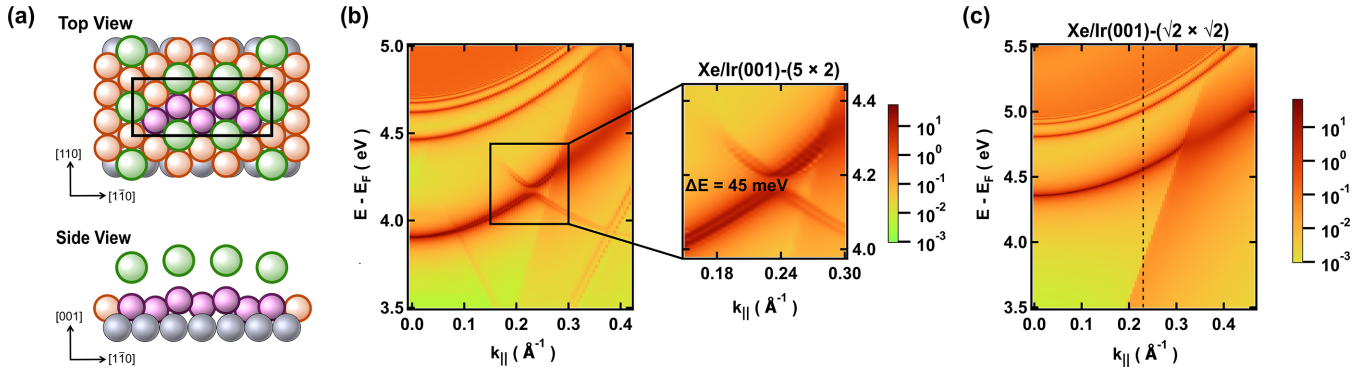

FIG. 4. (a) Ball model showing the top and side view for the Xe/(5×2) surface, with the unit cell marked by a black rectangular box. The Xe atoms are represented by green spheres. Calculated band structure for (b) the Xe/(5×2) surface and (c) the Xe/$(\sqrt{2}\times\sqrt{2})$ surface, determined along the $\bar{\Gamma}$-$\bar{X}$ direction. The band structure is shown in logarithmic intensity. The zoomed-in area in (b) highlights the band gap.

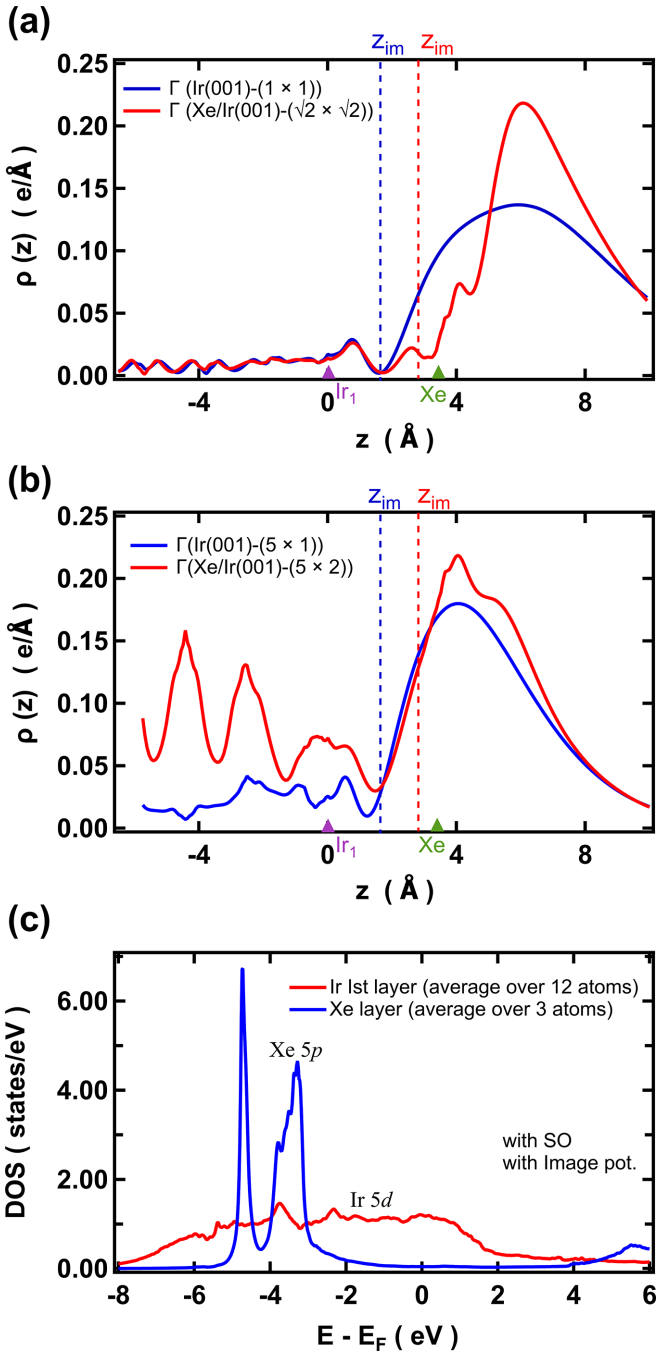

FIG. 5. Planar average charge density (ρ) distribution at the Γ point of the IPS state for (a) the clean Ir(001)-(1×1) surface (blue) and the Xe/($\sqrt{2}\times\sqrt{2}$) surface (red). (b) The charge density for the clean Ir(001)-(5×1) surface (blue) and the Xe/(5×2) surface (red). In both (a) and (b), the image plane (z_{im}) position for each structure is shown by red and blue dashed lines, respectively. In addition, the position of the topmost Ir (Ir1) and Xe atoms are marked by the purple and green triangles, respectively. (c) Calculated integrated density of states (DOS) projected onto the Xe adatoms (blue) and the Ir atoms (red) in the reconstructed topmost Ir layer of the Xe/Ir(001)-(5×1) surface.

significantly affect the charge density distribution of the IPS on the unreconstructed surfaces.

Figure 5(b) shows the planar-averaged charge density distributions at the $\bar{\Gamma}$ point of the IPS ($n = 1$) for the Xe-free (5×1) surface (blue curve) and the Xe/(5×2) surfaces (red curve). Regarding the Xe-covered surface, the IPS at $\bar{\Gamma}$ is located within a projected bulk band, and the charge-density oscillations in the interior of the Ir substrate seen in Fig. 5(b) arise from the bulk states in the same energy range and are not due to the IPS. It is technically not possible to extract only the charge density of the IPS from the calculated Green's function. By comparing the charge densities in Figs. 5(a) and 5(b), we observe that the charge density maxima move closer to the metal surface in the reconstructed surfaces than the unreconstructed ones. This may occur because the reconstructed surface has a 20% higher atomic density than the unreconstructed one, which results in higher electron densities and the more attractive exchange-correlation one-electron potential at the surface. Again, z_{im} position for Xe-covered surface (red dashed line) is located at the interior of the topmost Xe layer. The overall shape of the blue and red curves are very similar, except for a shoulder in the red curve at z ≈ 5.15 Å, which is attributed to the charge density from the Xe atoms. The nearly identical position of the charge density maxima across both curves confirm that Xe adsorption has a minor effect on the charge distribution of the IPS, especially on the reconstructed surfaces.

While one might expect Xe adsorption to significantly shift the charge density maxima away from the Ir surface, this is not observed. Two major factors may contribute to this behavior: the positive electron affinity of Xe and the image plane position with respect to the Xe overlayer.

Previous studies have demonstrated that the interaction between a metal surface and a dielectric layer induces charge redistribution across the interface, creating a dipole that shifts the Fermi level (E_F) in the metal [29,52,60,61] and polarizes the Xe atoms [62]. The positive electron affinity of Xe plays a crucial role in its interaction with the IPS. Unlike materials with negative electron affinity, such as Ar, which provide a repulsive barrier and push the IPS wave function toward the vacuum region [63], the positive electron affinity of Xe weakens the screening effect. The reduced screening allows partial penetration of the IPS wave function into the Xe layer [15,64]. As a result, the charge density remains largely unaffected, with the IPS still strongly bound near the surface.

The z_{im} position observed for the Xe-covered surfaces further supports these results. The image planes of low-index surfaces of elemental metals are typically located at 1–2 Å on the vacuum side of the topmost lattice plane [40,42,43]. For clean Ir(001), our DFT calculation yielded $z_{im} = 1.59$ Å for the (1×1) surface and $z_{im} = 1.63$ Å as measured from the averaged z coordinate of the corrugated reconstructed layer for the (5×1) surface. Similarly, in the jellium model, where the nuclear charge is treated as the uniform positive background charge, the z_{im} is not located exactly at the edge of this uniform background but is displaced by approximately 0.6–0.8 Å toward the vacuum, depending on the bulk electron density parameter [40,42,43]. However, for the Xe-covered surfaces, the image plane is located at the interior of the Xe layer, indicating that the shift of z_{im} by Xe adsorption is less than expected. This can be attributed to the dielectric nature of the Xe layer, which weakens the strength of the image force compared to the clean metal surface, limiting its ability to push z_{im} further away from the surface [62]. It indicates that

Xe is less polarized than the Ir substrate. To further support this argument, we calculated the integrated density of states (DOS) for the Xe-covered (5×2) surface. The blue and red lines in Fig. 5(c) show the DOS projected on the Xe adatoms and Ir atoms in the reconstructed Ir topmost layer, respectively. Within linear response theory, the screening charge induced by an external field is created by electronic states near the Fermi level. The nearly vanishing DOS near the Fermi level of the Xe atoms shown in Fig. 5(c) indicates that the Xe overlayer cannot screen the external field effectively. Therefore, the image plane position is located at the interior of the topmost Xe layer.

The combination of weak positive electron affinity and dielectric screening explains why the charge density distribution remains unchanged after the Xe adsorption. Since the charge density distribution of the IPS remains nearly unchanged in their position relative to the reconstructed surface after Xe adsorption, the in-plane potential also remains largely unaffected. Therefore, we conclude that the band gap observed in the IPS is an intrinsic feature of the Ir(001) caused by surface reconstruction and not significantly influenced by the Xe adsorption.

Finally, we comment on the possible role of Xe-induced effects beyond simple work function modulation. As discussed by Güdde and Höfer [15], rare-gas layers can introduce buried image-potential-like interface states or modify the IPS via electrostatic potential corrugation. These effects are more prominent in thicker layers with negative electron affinity gases. In contrast, we use only monolayer Xe of positive electron affinity and our DFT results do not show the interface states. Furthermore, the energy gap is observed even without Xe, reinforcing that the gap originates from the underlying (5×1) reconstruction rather than any hybridization or interface-localized states. We thus conclude that the monolayer Xe serves primarily to reduce the work function and plays no essential role in the origin of the band gap. It would be interesting to detect buried interface states by using a thicker Xe sample.

IV. CONCLUSION

In this study, we investigated the impact of surface reconstruction on the IPSs using the unreconstructed and the reconstructed Ir(001) surfaces by 2PPE spectroscopy and DFT calculations. Our 2PPE results experimentally revealed the band gap in the IPS of the Xe/Ir(001)-(5×1) surface, which was absent in the Xe/Ir(001)-(1×1) surface. This band gap in the unoccupied state is caused by the change in the potential distribution due to surface reconstruction. DFT calculations confirmed that the band gap persists in the reconstructed surface with or without Xe adsorption. The results of this work demonstrate the robustness of surface reconstruction as a tool for tuning the unoccupied states.

ACKNOWLEDGMENTS

This work was financially supported by JSPS KAKENHI (Grant No. 22H01960) and the World Premier International Research Center Initiative (WPI) on Materials Nanoarchitectonics, MEXT, Japan. It is also partially supported by the National Science and Technology Council, Taiwan under NSTC 114–2923-M-A49-001-MY2, NSTC 113–2124-M-A49-007, NSTC 113–2628-M-A49-006-MY3, and NSTC T-Star Center Project: Future Semiconductor Technology Research Center under NSTC 114–2634-F-A49-001.

DATA AVAILABILITY

The data that support the findings of this article are not publicly available upon publication because it is not technically feasible and/or the cost of preparing, depositing, and hosting the data would be prohibitive within the terms of this research project. The data are available from the authors upon reasonable request.

[1] T. N. Rhodin and G. Brodén, Preparation and chemisorptive properties of the clean normal and reconstructed surfaces of Ir(100)—role of multiplets, Surf. Sci. **60**, 466 (1976).

[2] D. Spišák and J. Hafner, Reconstruction and de-reconstruction of the Ir(1 0 0) surface and ultrathin Fe/Ir(1 0 0) Films, Surf. Sci. **546**, 27 (2003).

[3] A. Nuber, M. Higashiguchi, F. Forster, P. Blaha, K. Shimada, and F. Reinert, Influence of reconstruction on the surface state of Au(110), Phys. Rev. B **78**, 195412 (2008).

[4] N. Memmel, Monitoring and modifying properties of metal surfaces by electronic surface states, Surf. Sci. Rep. **32**, 91 (1998).

[5] A. Bendounan, H. Cercellier, Y. Fagot-Revurat, B. Kierren, V. Y. Yurov, and D. Malterre, Modification of shockley states induced by surface reconstruction in epitaxial Ag films on Cu(111), Phys. Rev. B **67**, 165412 (2003).

[6] P. M. Echenique and J. B. Pendry, The existence and detection of rydberg states at surfaces, J. Phys. C: Solid State Phys. **11**, 2065 (1978).

[7] P. M. Echenique and J. B. Pendry, Theory of image states at metal surfaces, Prog. Surf. Sci. **32**, 111 (1989).

[8] Y. Zhang, Z. Yang, X. Zhang, B. Lin, G. Lin, and J. Chen, Coulomb-coupled quantum-dot thermal transistors, Europhys. Lett. **122**, 17002 (2018).

[9] F. Craes, S. Runte, J. Klinkhammer, M. Kralj, T. Michely, and C. Busse, Mapping image potential states on graphene quantum dots, Phys. Rev. Lett. **111**, 056804 (2013).

[10] Y. Zhang, Q. Chen, A. P. Alivisatos, and M. Salmeron, Dynamic charge carrier trapping in quantum dot field effect transistors, Nano Lett. **15**, 4657 (2015).

[11] Q. Wang *et al.*, Ultrafast broadband photodetectors based on three-dimensional dirac semimetal Cd_3As_2, Nano Lett. **17**, 834 (2017).

[12] K. Wandelt and J. E. Hulse, Xenon adsorption on palladium. I. the homogeneous (110), (100), and (111) Surfaces, J. Chem. Phys. **80**, 1340 (1983).

[13] J. L. F. Da Silva, C. Stampfl, and M. Scheffler, Xe adsorption on metal surfaces: First-principles investigations, Phys. Rev. B **72**, 075424 (2005).

[14] J. L. F. de Silva, C. Stampfl, and M. Scheffler, Adsorption of Xe atoms on metal surfaces: New insights from first-principles calculations, Phys. Rev. Lett. **90**, 066104 (2003).
[15] J. Güdde and U. Höfer, Femtosecond time-resolved studies of image-potential states at surfaces and interfaces of rare-gas adlayers, Prog. Surf. Sci. **80**, 49 (2005).
[16] T. Yamada, N. Kawakita, C. Okui, and T. Munakata, Hybridization of an unoccupied molecular orbital with an image potential state at a lead phthalocyanine/graphite interface, J. Phys.: Condens. Matter **31**, 044004 (2018).
[17] B. W. Caplins, A. J. Shearer, D. E. Suich, E. A. Muller, and C. B. Harris, Measuring the electronic corrugation at the metal/organic interface, Phys. Rev. B **89**, 155422 (2014).
[18] N. Armbrust, J. Güdde, P. Jakob, and U. Höfer, Time-resolved two-photon photoemission of unoccupied electronic states of periodically rippled graphene on Ru(0001), Phys. Rev. Lett. **108**, 056801 (2012).
[19] X. Wang, X. Shen, R. Osgood, R. Haight, and F. Himpsel, Observation of lateral superlattice effects on stepped Cu(001), Phys. Rev. B **53**, 15738 (1996).
[20] I. G. Hill and A. B. Mc Lean, Strongly anisotropic band dispersion of an image state located above metallic nanowires, Phys. Rev. Lett. **82**, 2155 (1999).
[21] S. Bode, K. Starke, P. Rech, and G. Kaindl, Highly spin-polarized, nearly free-electron states in front of Co(10$\bar{1}$0), Phys. Rev. Lett. **72**, 1072 (1994).
[22] E. A. Muller, J. E. Johns, B. W. Caplins, and C. B. Harris, Quantum confinement and anisotropy in thin-film molecular semiconductors, Phys. Rev. B **83**, 165422 (2011).
[23] X. Cao *et al.*, Revisiting oxygen adsorption on Ir(100), J. Phys. Chem. C **126**, 10035 (2022).
[24] A. Ignatiev, A. V. Jones, and T. N. Rhodin, Leed investigations of xenon single crystal films and their use in studying the Ir(100) surface, Surf. Sci. **30**, 573 (1972).
[25] K. Anic, A. V. Bukhtiyarov, H. Li, C. Rameshan, and G. Rupprechter, CO adsorption on reconstructed Ir(100) surfaces from UHV to mbar pressure: A LEED, TPD, and PM-IRAS Study, J. Phys. Chem. C **120**, 10838 (2016).
[26] K. Heinz, G. Schmidt, L. Hammer, and K. Müller, dynamics of the reconstruction process Ir(100) $1\times1 \rightarrow 1\times5$, Phys. Rev. B **32**, 6214 (1985).
[27] A. Schmidt, W. Meier, L. Hammer, and K. Heinz, deep-going reconstruction of Ir(100)-5×1, J. Phys.: Condens. Matter **14**, 12353 (2002).
[28] J. Ross Macdonald and C. A. Barlow, Work function change on monolayer adsorption, J. Chem. Phys. **39**, 412 (1963).
[29] K. Wandelt, The local work function: Concept and implications, Appl. Surf. Sci. **111**, 1 (1997).
[30] T. Fauster and W. Steinmann, in *Electromagnetic Waves: Recent Developments in Research*, 1st ed. (Elsevier, Amsterdam, 1995), Vol. 2, Chap. 8, pp. 347–411.
[31] N. D. Lang and W. Kohn, Theory of metal surfaces: Work function, Phys. Rev. B **3**, 1215 (1971).
[32] J. Küppers, H. Michel, F. Nitschké, K. Wandelt, and G. Ertl, Xenon adsorption as a tool for local surface structure determination at Ir(100) surfaces, Surf. Sci. **89**, 361 (1979).
[33] H. Ishida, Surface-embedded green-function method: A formulation using a linearized-augmented-plane-wave basis set, Phys. Rev. B **63**, 165409 (2001).
[34] J. E. Inglesfield, A method of embedding, J. Phys. C Solid State Phys. **14**, 3795 (1981).
[35] D. J. Singh and L. Nordstrom, *Planewaves, Pseudopotentials, and the LAPW Method* (Springer Science & Business Media, New York, 2006).
[36] H. Ishida, Rashba spin splitting of shockley surface states on semi-infinite crystals, Phys. Rev. B **90**, 235422 (2014).
[37] T. Nakazawa, N. Takagi, M. Kawai, H. Ishida, and R. Arafune, Rashba splitting in an image potential state investigated by circular dichroism two-photon photoemission spectroscopy, Phys. Rev. B **94**, 115412 (2016).
[38] H. Ishida, Surface band structure of the reconstructed Ir(001)-(5×1) surface, Surf. Sci. **744**, 122472 (2024).
[39] M. Nekovee, Theory of image states at magnetic surfaces, Prog. Surf. Sci. **50**, 149 (1995).
[40] N. D. Lang and W. Kohn, Theory of metal surfaces: Induced surface charge and image potential, Phys. Rev. B **7**, 3541 (1973).
[41] N. D. Lang, Interaction between closed-shell systems and metal surfaces, Phys. Rev. Lett. **46**, 842 (1981).
[42] R. O. Jones, P. J. Jennings, and O. Jepsen, Surface barrier in metals: A new model with application to W(001), Phys. Rev. B **29**, 6474 (1984).
[43] P. J. Jennings, R. O. Jones, and M. Weinert, Surface barrier for electrons in metals, Phys. Rev. B **37**, 6113 (1988).
[44] G. Kresse and J. Hafner, *Ab initio* molecular dynamics for liquid metals, Phys. Rev. B **47**, 558 (1993).
[45] G. Kresse and J. Furthmüller, Efficiency of *ab-initio* total energy calculations for metals and semiconductors using a plane-wave basis set, Comput. Mater. Sci. **6**, 15 (1996).
[46] J. Klimeš, D. R. Bowler, and A. Michaelides, Van Der Waals density functionals applied to solids, Phys. Rev. B **83**, 195131 (2011).
[47] I. Hamada, Van Der Waals density functional made accurate, Phys. Rev. B **89**, 121103 (2014).
[48] P. Zhang, P. Richard, T. Qian, Y.-M. Xu, X. Dai, and H. Ding, A precise method for visualizing dispersive features in image plots, Rev. Sci. Instrum. **82**, 043712 (2011).
[49] T. Nakazawa, R. Arafune, N. Takagi, and M. Kawai, Linewidth analysis of image potential states on noble metal surfaces with high-energy resolved two-photon photoemission spectroscopy, Surf. Interface Anal. **48**, 1194 (2016).
[50] See Supplemental Material at http://link.aps.org/supplemental/10.1103/46k5-fft2 for details on the parabolic fitting of the IPS on the Xe/(1×1) surface and the band structure calculation using the Kronig-Penney model for the Ir(001)-(5×1) surface.
[51] R. D. L. Kronig and W. G. Penney, Quantum mechanics of electrons in crystal lattices, Proc. R. Soc. London Ser. A **130**, 499 (1931).
[52] K. Wandelt, *Surface and Interface Science* (John Wiley & Sons, Hoboken, NJ, 2016), Vol. 5.
[53] C. Hückstädt, S. Schmidt, S. Hüfner, F. Forster, F. Reinert, and M. Springborg, Work function studies of rare-gas/noble metal adsorption systems using a kelvin probe, Phys. Rev. B **73**, 075409 (2006).
[54] G. Butti, S. Caravati, G. P. Brivio, M. I. Trioni, and H. Ishida, Image potential states and electronic structure of Na/Cu(111), Phys. Rev. B **72**, 125402 (2005).

[55] M. A. Van Hove, R. J. Koestner, P. C. Stair, J. P. Bibérian, L. L. Kesmodel, I. Bartoš, and G. A. Somorjai, The surface reconstructions of the (100) crystal faces of iridium, platinum and gold. II. structural determination by LEED intensity analysis, Surf. Sci. **103**, 218 (1981).

[56] H. C. Poon, D. K. Saldin, D. Lerch, W. Meier, A. Schmidt, A. Klein, S. Müller, L. Hammer, and K. Heinz, Spontaneous symmetry breaking of the Ir(100)-(5×1)-Hex surface induced by hydrogen adsorption, Phys. Rev. B **74**, 125413 (2006).

[57] G. Gilarowski, J. Méndez, and H. Niehus, Initial growth of Cu on Ir(100)-(5×1), Surf. Sci. **448**, 290 (2000).

[58] H. Ishida, R. Arafune, and N. Takagi, First-principles calculation of the graphene dirac band on semi-infinite Ir(111), Phys. Rev. B **102**, 195425 (2020).

[59] This structure is a hypothetically assumed model and cannot be realized in practice because the lattice constant of the Xe lattice becomes shorter than that of the close-packed Xe Lattice.

[60] S. Prada, U. Martinez, and G. Pacchioni, Work function changes induced by deposition of ultrathin dielectric films on metals: A theoretical analysis, Phys. Rev. B **78**, 235423 (2008).

[61] T. Engel and R. Gomer, Adsorption of inert gases on tungsten: Measurements on single crystal planes, J. Chem. Phys. **52**, 5572 (1970).

[62] W. R. Merry, R. E. Jordan, D. F. Padowitz, and C. B. Harris, Electrons at metal-insulator interfaces: I. The effect of Xe monolayers on the image potential states of Ag(111), Surf. Sci. **295**, 393 (1993).

[63] P. M. Echenique, R. Berndt, E. V. Chulkov, T. Fauster, A. Goldmann, and U. Höfer, Decay of electronic excitations at metal surfaces, Surf. Sci. Rep. **52**, 219 (2004).

[64] W. Berthold, F. Rebentrost, P. Feulner, and U. Höfer, Influence of Ar, Kr, and Xe layers on the energies and lifetimes of image-potential states on Cu(100), Appl. Phys. A **78**, 131 (2004).